Journal of
Materials Chemistry B

Accepted Manuscript

ROYAL SOCIETY OF CHEMISTRY

www.rsc.org/materialsB

Dextran-coated fluorapatite nanorods doped with lanthanides in labelling and directing osteogenic differentiation of bone marrow mesenchymal stem cells

Haifeng Zeng[a], Xiyu Li[b], Fang Xie[a], Li Teng[a*], and Haifeng Chen[b**]

[a] Cranio-Maxillo-Facial Surgery Department 2, Plastic Surgery Hospital of Peking Union Medical College & Chinese Academy of Medical Sciences, Beijing 100144, P.R. China

[b] Department of Biomedical Engineering, College of Engineering, Peking University, Beijing 100871, P.R. China

* Corresponding author. Tel.: +86 010 88771519.

** Corresponding author. Tel: + 86 010 62754396.

E-mail addresses: zhengxingwuke@163.com (Li Teng), haifeng.chen@pku.edu.cn (Haifeng Chen)

Abstract

Terbium (Tb)- or europium (Eu)-doped fluorapatite nanorods (Tb/Eu-FHA) were prepared using the hydrothermal method. The structure, morphology, and luminescence of the products were determined using X-ray diffraction (XRD), field emission scanning electron microscopy (ESEM), transmission electron microscopy (TEM), and photoluminescence spectra (PL). The surfaces of the Tb/Eu -FHA nanorods were further conjugated with hydrophilic cationic polymers, such as dextran, to enhance hydrophilicity, biocompatibility and cell penetration. Then, the dextran-coated nanorods were cocultured with bone marrow mesenchymal stem cells (BMSCs). A luminescence signal in the cells was detected after 12 hours with a laser scanning confocal microscope (LSCM). Labelled BMSCs were shown to reproducibly exhibit osteogenic differentiation potential in real-time PCR and ELISA assays. *In vivo* cell-tracking experiments also suggested that dextran-coated Tb-FHA nanorods could be used as a stable tracer of BMSCs. Therefore, dextran-coated Tb-FHA nanorods can be utilised for tracking and monitoring BMSCs *in vitro* and *in vivo*. Our current work attempts to provide an excellent fluorescent cell labelling agent for BMSCs in bone tissue engineering.

Keywords: Fluorapatite; Fluorine-substituted hydroxyapatite; Cell tracking; Bone mesenchymal stem cells; Lanthanides

As a major inorganic ingredient of bone and teeth, hydroxyapatite [HA, $Ca_{10}(PO_4)_6(OH)_2$] has been used in a broad range of biomedical applications, such as orthopaedic implant coating, local drug delivery and gene transfection. The nanophase hydroxyapatite possesses superior surface properties and energetics compared with its bulk phase counterpart.[1] The high surface-to-volume ratio, reactivities, and biocompatibility of nanophase hydroxyapatite provide a more favourable synthetic microenvironment that closely mimics natural bone tissue physiology. When hydroxyapatite nanorods are doped with lanthanides (Eu^{3+} Tb^{3+} or Gd^{3+}), the nanorods can obtain special photoluminescent and magnetic multifunctions. The complexes have great potential in applications of imaging agents for magnetic resonance imaging (MRI), photoluminescence imaging and computed tomography imaging (CT).[2] However, in the early stage, fluorescent hydroxyapatite nanorods doped with lanthanides demonstrated flaws in crystallinity, size uniformity and an agglomerate dispersed state in solution.[3,4] These disadvantages limit the biomedical applications of hydroxyapatite nanorods in living cells. Some scholars tend to integrate HA with fluorescein isothiocyanate (HA-FITC) because of its favourable biocompatibility and cell labelling capability.[5] However, fluorescein isothiocyanate (FITC) demonstrates a short quenching time and poor light stability. Some inorganic dyes, such as quantum dots (QDs), show a long quenching time and good light stability; however, they also demonstrate high toxicity to living organisms due to their heavy metal ions (e.g., Cd^{2+}).[6,7]

Monodisperse hydroxyapatite nanorods synthesised *via* a hydrothermal synthetic route based on the liquid-solid-solution (LSS) strategy exhibit excellent luminescent properties with the doping of Ln^{3+} (Eu^{3+} or Tb^{3+}) ions. The luminescent nanorods have been reported to label HeLa cells and A549 cells.[8,9] R Sun. *et. al* claimed that Eu-doped fluorine-substituted hydroxyapatite (Eu-FHA) nanorods synthesised using a simple hydrothermal method do not adversely affect the growth of HeLa cells, which indicates that the nanorods have potential applications as fluorescent cell labelling agents.[10]

Fluorapatite nanorods (FHA, FA) are also called fluoride-substituted hydroxyapatite or fluor-hydroxyapatite. The -OH groups in the lattice are replaced by F^- ions to further enhance the fluorescence of the Ln^{3+} ions and give rise to the quenching of the excited state.[11,12] Rich super-hydrophobic oleic acid molecules on the surface of the nanorods inhibit their biological applications. Thus, the hydrophobic fluoridated nanorods must be converted into hydrophilic nanorods *via* surface modifications or by coating with surfactant Pluronic F127, PEG or another cationic polymer.

Dextran is a complex branched glucan (polysaccharide made of many glucose molecules) composed of chains lengths varying from 3 to 2000 kilodaltons and is widely used in laboratory research. Dextran is a type of stable coating to protect metal nanoparticles from oxidation and to improve the biocompatibility of many materials, such as superparamagnetic iron oxide nanoparticles, gold nanoparticles, cerium oxide nanoparticles and quantum dots.[13-16] Most dextran-coated nanoparticles exhibit excellent antioxidant properties as well as high biocompatibility and stability properties. The hydrolysate of dextran is glucan, which is the basic component of nutrition and is harmless to animal cells. BMSCs are favourable seed cells in bone tissue engineering; however, an ideal tracer for BMSCs remains elusive. In this study, we used dextran-coated luminescent fluorapatite nanorods doped with lanthanides (15%Tb^{3+}) to label and track canine BMSCs (cBMSCs) and to explore the influence of luminescent fluorapatite nanorods on BMSC viability and differentiation.

Materials and methods

All animal and experimental procedures were approved by the Institutional Animal Care Committee and the Committee of the Plastic Surgery Hospital (Institute) and complied with the "Guide for the Care and Use of Laboratory Animals" published by the National Academy Press (NIH Publication No. 85-23, revised 1996).

Cell cultures

Bone marrow aspirates were harvested from the anterior superior iliac spine of beagle dogs and then rushed into 50-mL tubes. They were centrifuged at 1300 rpm for 3 minutes, and the pellets were suspended in Dulbecco's modified Eagle's low glucose medium (DMEM; HyClone, America) supplemented with 10% foetal bovine serum (FBS; Sigma, America), 2 mM l-glutamine (Sigma America), 100 U/mL penicillin and 100 μg/mL streptomycin sulphate (HyClone, America). The cells were plated in 100-mm culture dishes with supplemented DMEM and maintained in a 5% CO2 atmosphere at 37 ℃. The medium was changed after 48 hours. When the cells reached 80–90% confluence, they were detached with 0.25% trypsin/EDTA (Gibco, America) and subcultured at a density of 1 × 105 cells/cm^2 in 100-mm dishes. The medium was replaced three times per week. All experiments were performed on second- or third- passage cells.

Identification of the characteristics of canine BMSCs

The specific cell surface antigen markers of cBMSCs were examined using flow cytometry (FCM, BD, America). Canine bone marrow-derived mesenchymal stem cells exhibit high expressions of CD29 and CD44 and are negative for CD34 and CD45.[17] The antibodies for positive markers included CD29 (Abcam, ab64629, Britain) and CD44 (Abcam, ab119863, Britain), whereas those for the negative markers included CD34 (Abcam, ab24055, Britain) and CD45 (Abcam, ab22514, Britain).

Preparation of dextran-coated Tb/Eu-FHA nanorods

Eu^{3+} or Tb^{3+} -doped FHA nanorods were synthesised *via* the hydrothermal method. Octadecylamine (0.5 g) was dissolved in 4 mL of oleic acid by heating; 16 mL of ethanol and an aqueous solution of $Ca(NO_3)_2$ (0.28 M, 7 mL) were then added. The mixture was stirred for 3 min, then NaF (0.24 M, 2 mL) and Na_3PO_4 (0.168 M, 7 mL) were added to the solution. The mixture was stirred for an additional

5 min, sealed, and maintained at a controlled temperature (150 ℃) for 12 h. Lastly, $Eu(NO_3)_3$ or $Tb(NO_3)_3$ (0.28 M, 2.8 mL) were added to the mixture; it was then stirred for 5 min and treated at a controlled temperature (160 ℃) for 16 h.

Characterisation of Tb/Eu-FHA nanorods

Transmission electron microscopy (TEM) was performed using a FEI Tecnai G2 T20 instrument at 200 KV to measurement the sizes and morphologies of the FHA doped with Eu^{3+} or Tb^{3+} nanoparticles. Samples were prepared by placing a drop of a diluted ethanol dispersion of the products on the surface of a copper grid. XRD analysis was performed using Philips X' Pert Pro MPD in the 2θ range from 10° to 65° with Cu Kα radiation (λ = 1.5406 Å). Luminescence spectra were recorded with a Hitachi F-4500 fluorescence spectrophotometer. Luminescent photography of the samples was performed under UV light at 395 nm.

Dextran grafting on Tb/Eu-FHA nanorods.

The obtained FHA nanorods doped with Eu^{3+} or Tb^{3+} were collected *via* centrifugation and washed thrice using ethanol. The prepared nanorods were dispersed in cyclohexane (5 mL) and mixed with a dextran solution (100 mg, 10 mL).Then, 10 mL of tetrahydrofuran was added to the mixture. The mixture was dispersed *via* ultrasonication and stirred for 2 h at room temperature. Lastly, it was isolated *via* centrifugation and purified with ethanol three times.

Cell proliferation assay

cBMSCs cells were seeded in 96-well microplates at a density of 1 x 10^5 cells mL^{-1} and cultured for 24, 48, and 72 h in media containing Tb/Eu-THA nanorods at concentrations of 50 μg mL^{-1}, 100 μg mL^{-1} and 200 μg mL^{-1}, respectively. BMSC cell viability was evaluated using a tetrazolium compound assay (MTS, G3580, Promega, Australia). The plates were analysed using a microplate reader (Enspire, PerkinElmer, America). Measurements of the MTS dye absorbance were performed at 490 nm. Three replicate wells were used per microplate, and the experiments were repeated three times. Cell survival was expressed as the absorbance relative to the untreated controls. The results were presented as the means ± standard deviation.

Microstructure observation

The cBMSCs and the dextran-coated Tb/FHA at a concentration of 100 μg mL^{-1} were coculture in glass dishes for more than 12 h. Fluorescent images of cBMSCs incubated with dextran-coated Tb/Eu-THA nanorods were performed *via* LSCM (LSM780, Zeiss, German); the excited wavelengths utilised were 405 nm and 488 nm. ESEM images were performed using FEI Quanta 250.

Real-time polymerase chain reaction

The mRNA levels of alkaline phosphatase (ALP), the alpha l chain of type I collagen (COL1α1), and Osteonectin (ON) mRNA were analysed *via* real-time PCR assay on days 14 and 21 of differentiation. TRIzol reagent (Invitrogen, USA) was used to extract the total RNA from the cells according to the manufacturer's protocol. The real-time PCR primers (synthesised by Sangon, Shanghai, China) were ALP 5'-agctcatgcacaacgtcaag-3', 5'-gtgcttgtgtctcggtttga-3'; Col Iα1: 5'-acagccgcttcacctacagt-3', 5'-atatccatgccgaattcctg-3'; ON: 5'-ggtccttgccctgctggctg-3', 5'-ccgggccatagaagcgctgg-3'; and glyceraldehyde-3- phosphate dehydrogenase (GAPDH), 5'-atcaccatcttccaggag-3', 5'-atcgactgtggtcatgag-3'. Real-time PCR method was performed by Takara PCR reagent (Takara code: DRR420a).

ELISA essays

The ALP activity was detected using ALP spectrophotometry on days 14 and 21 of differentiation. The supernatants of the culture dishes were collected and centrifuged at 3000 rpm for 10 min at 4℃ to

remove debris. They were then assessed for ALP using an ALP Kit (Walan, Shanghai, China) according to the manufacturer's instructions. The absorbance was found to be 490 nm using a PerkinElmer instrument.

***In vivo* observation**

A highly porous PCL scaffold was fabricated as a 5 mm ×5 mm ×5 mm cube with an inclined groove. The labelled BMSCs were seeded on sterilised PCL scaffold in a concentration of 1×10^7 cells/ml, were 3D-cultured for 3 days prior to implantation, and were then implanted subcutaneously into nude mice. Six nude mice were randomly divided into two groups (1 month and 3 months groups, n = 3 in each group). Samples were harvest at 1 and 3 months. Specimens were used to make rapid frozen sections that were then stained with haematoxylin and eosin (HE). Images were collected *via* inverted fluorescence microscope (TE2000, Nikon, Japan).

Statistical analysis

The statistical analysis was performed using SPSS 13.0 software. Student's t-test was performed to determine the statistical significance between the experimental groups. $P < 0.05$ was considered to indicate statistical significance. All of the results are expressed as the means ±standard deviation.

Results and discussion

cBMSC cultures and characterisation

All characterisations were performed on cells of passage 2 or 3. After isolation and expansion, all cBMSCs had a homogeneous phenotype. FCM results show that the cBMSCs consisted of a single phenotypic population that was positive for CD29 (96.4%) and CD44 (99.3%). In contrast, these cells were negative for markers of the hematopoietic lineage, including the lipopolysaccharide receptor CD34 (3.65%) and the leukocyte common antigen CD45 (0.635%) (Fig. 1 A to D).

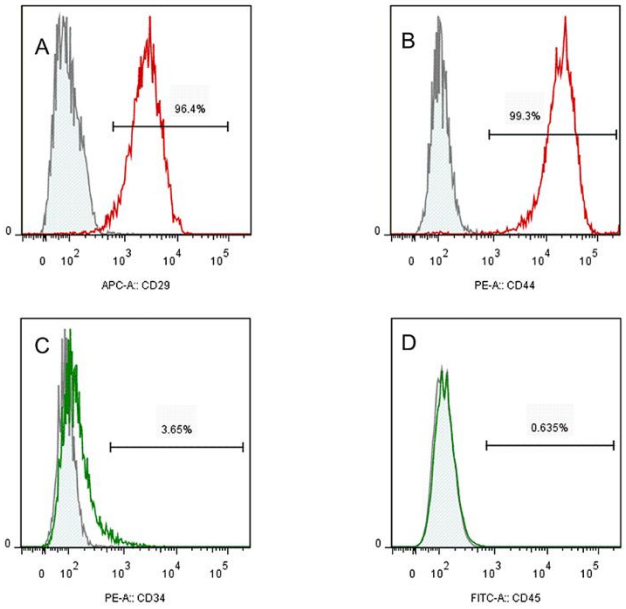

Fig. 1 Immunophenotype analysis of cBMSCs *via* flow cytometry. Positive markers of CD29 and CD44 are shown in A and B, and the negative markers of CD34 and CD45 are shown in C and D.

Characterisation of Tb/Eu-FHA nanorods

A typical TEM image of dextran-coated FHA nanorods doped with 15% Tb^{3+} is shown in Fig. 2A. The TEM image also shows that Tb-FHA nanorods are straight and rod-like, with a diameter of

approximately 15 to 20 nm and lengths ranging from 110 to 170 nm (Fig. 1B). The nanorods possess uniform morphology and good crystallinity. Fig. 2 C, D and E show the nanoparticle powders under UV light in an Eppendorf tube (C) and a converted fluorescence microscope (D and E). Fig. 3 describes the X-ray diffraction patterns for synthesised FHA nanorods doped with Tb^{3+} and Eu^{3+}; all diffraction peaks can be indexed as typical hexagonal FHA (ICDD 15-0876). The sharp characteristic peaks at approximately 25.9 ° and 32.0 ° correspond to (002) and (211) lattice planes. The hexagonal crystal structure of apatite has good stability, which would be helpful for the stable fluorescence expression of the embedded rare-earth ions. Fig. 4 shows that Tb-FHA nanorods become luminescent with a maximum emission intensity at 543 nm ($^5D_4$-$^7F_5$), and the emission intensity of Eu-FHA nanorods is 617 nm ($^5D_0$-$^7F_2$).

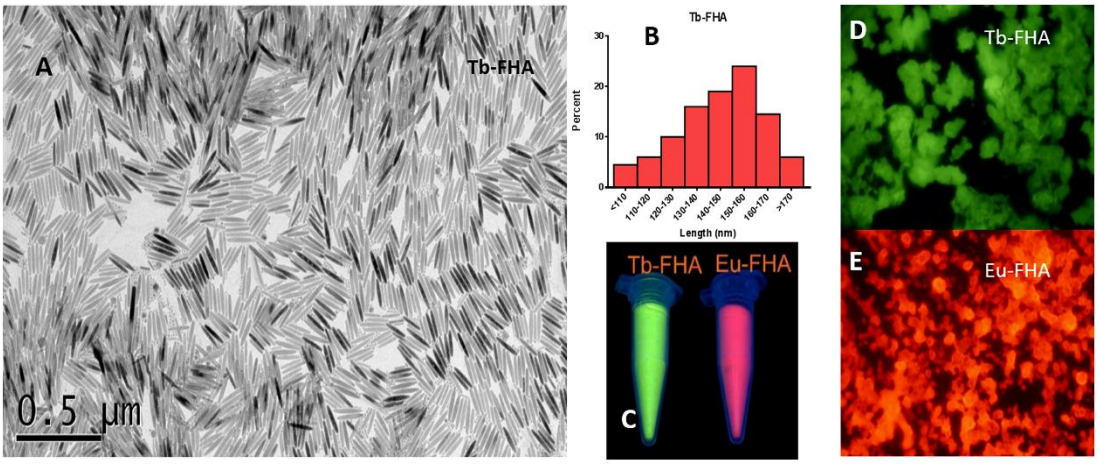

Fig. 2 TEM images of FHA nanoparticles doped with 15% Tb^{3+} nanorods (A), varying nanorod lengths (B), nanoparticle powders under UV light in an Eppendorf tube (C) and by using a converted fluorescence microscope (D, E).

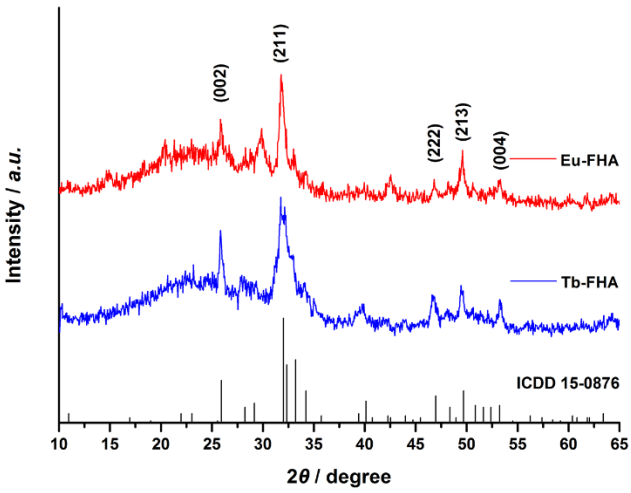

Fig. 3 X-ray diffraction patterns for synthesised Tb/Eu-FHA nanorods.

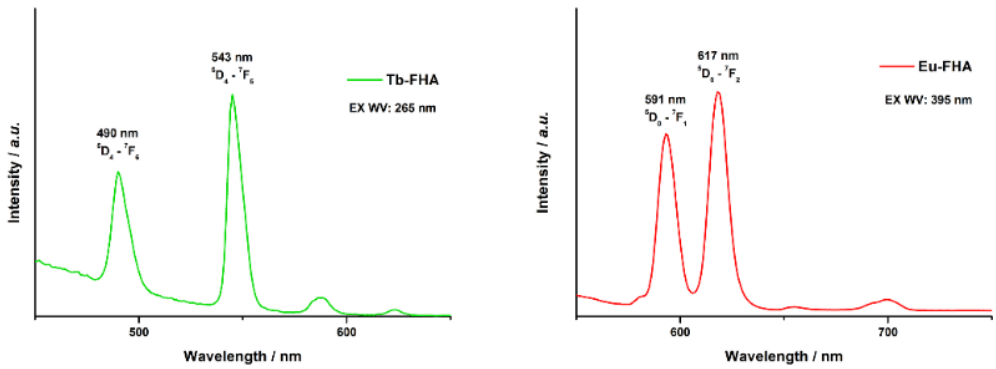

Fig. 4 The excite wavelength and emission spectra of Tb/Eu-FHA nanorods.

Biocompatibility of dextran-coated Tb/Eu-FHA nanorods

Fig. 5 shows the MTS result of cBMSCs cultured for 24, 48, and 72 h in media containing Tb/Eu-THA nanorods at concentrations of 50 μg mL^{-1}, 100 μg mL^{-1} and 200 μg mL^{-1}, respectively. No cytotoxicity was observed in the Tb-FHA group. The cell viability of the Eu-FHA group slightly decreases at a concentration of 200 μg mL^{-1}. The results demonstrate that dextran-coated FHA nanorods doped with Tb^{3+} or Eu^{3+} ions possess excellent biocompatibility.

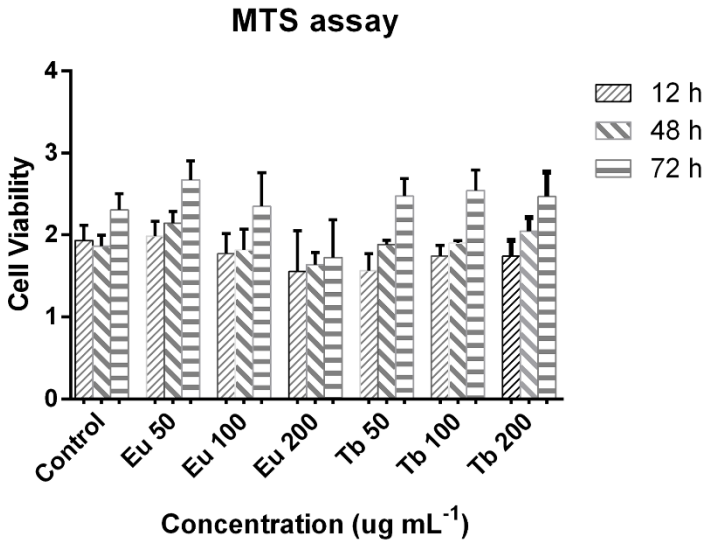

Fig. 5 Biocompatibility evaluation of dextran-coated Tb/Eu-THA nanorods. MTS assay of cBMSCs cultured for 24, 48, and 72 h in media containing Tb/Eu-THA nanorods at concentrations of 50 μg mL^{-1}, 100 μg mL^{-1} and 200 μg mL^{-1}, respectively.

Fluorescence microscopy image

The green/red fluorescence of cBMSCs is very clear in the Tb-FHA group and Eu-FHA group (Figure 6 and 7). The control group represents cBMSCs cultured in regular complete medium. Confocal images were recorded at an excitation wavelength of 488/405 nm; the green/red nanorods appeared to localise as discrete dots and to exhibit the morphology of the cells, which indicates that the nanorods have crossed the cell membrane and have been internalised.

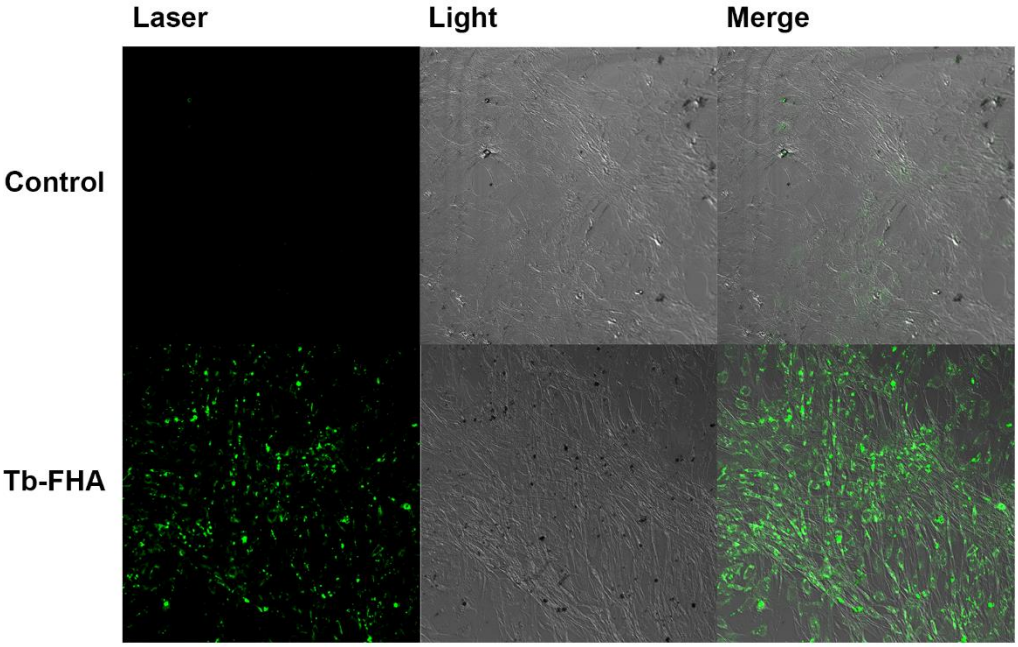

Fig. 6 LSCM images of cBMSCs incubated with dextran-coated Tb-FHA nanorods at a concentration of 100 μg mL^{-1} for 24 h. The control group is composed of cBMSCs that have been cultured in regular complete medium.

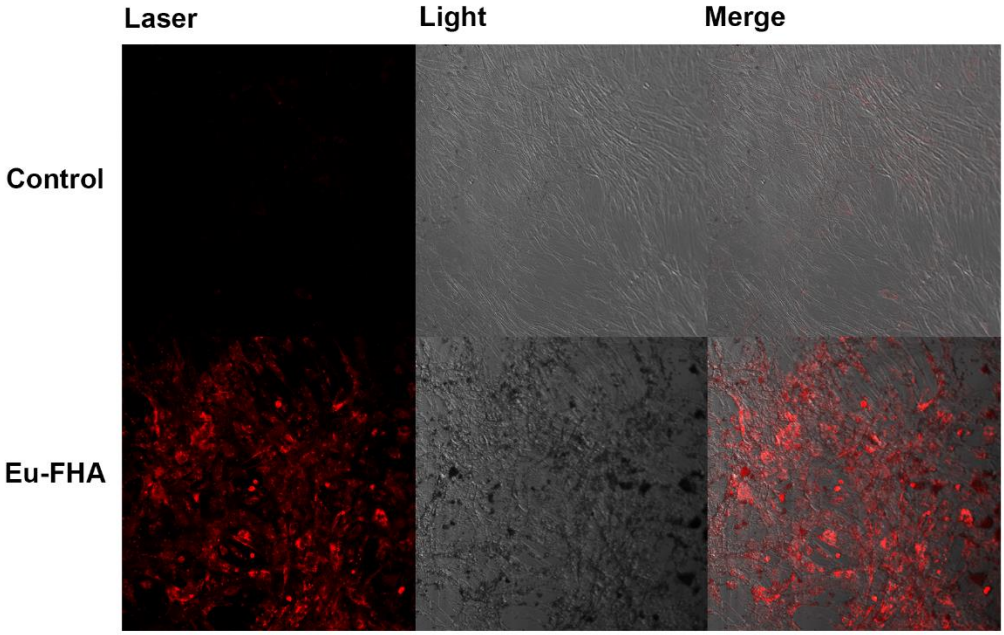

Fig. 7 LSCM images of cBMSCs incubated with dextran-coated Eu-THA nanorods at a concentration of 100 μg mL^{-1} for 24 h. The control group is composed of cBMSCs that have been cultured in regular complete medium.

Effects of Tb-FHA nanorods on the osteoblast-related gene expressions of cBMSCs

The mRNA levels of alkaline phosphatase (ALP), alpha l chain of type I collagen (COL1α1), and Osteonectin (ON) mRNA were analysed *via* real-time PCR assay on days 14 and 21 of differentiation. Fig. 8 shows the mRNA change of the relative gene expressions.

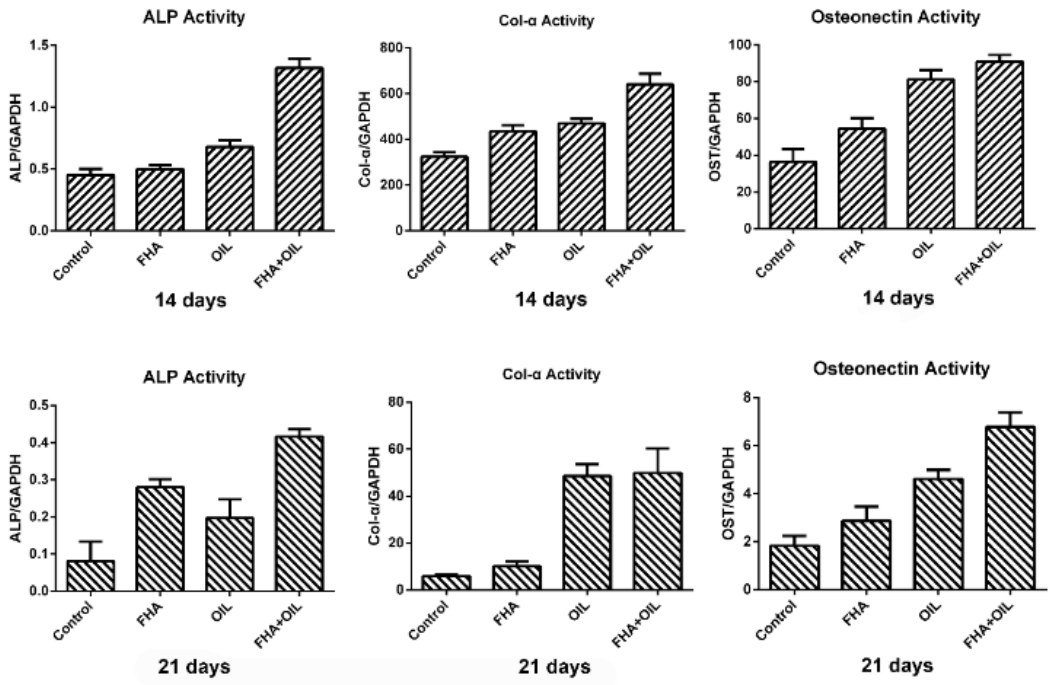

Fig. 8 Effects of the Tb-FHA nanorods on the osteoblast-related gene expressions of cBMSCs. Image analysis of (A, D) ALP, (B, E) Col-α and (C, F) ON gene expressions. The control group was treated with regular complete medium, the FHA group was treated with 100 μg mL^{-1} Tb-FHA with complete medium, the OIL group was treated with the osteogenesis induced liquid, and the FHA+OIL group was treated with both.

ALP ELISA assay

Fig. 9 shows the effect of the Tb-FHA nanorods on the osteoblast-related protein expression of cBMSCs. The ALP activity was detected *via* ALP spectrophotometry on days 14 (Fig. 9 A) and 21 (Fig. 9 B) of differentiation.

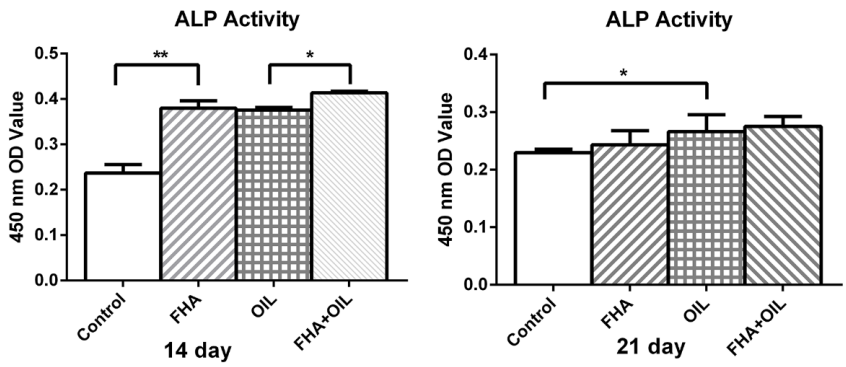

Fig. 9 Osteoblast-related protein expressions of Tb-FHA nanorods on cBMSCs. * indicates $P < 0.05$ and ** indicates $P < 0.01$.

***In vivo* implantation and intrinsic homing of the cBMSCs**

Labelled BMSCs were seeded on sterilised PCL scaffold that was subcutaneously implanted in nude mice. Samples were harvested 1 month (Fig. 10 A, B) and 3 months (Fig. 10 C, D) later, respectively.

Fluorescent images of the rapidly frozen sections were gathered *via* inverted fluorescence microscope; B shows image staining *via* haematoxylin and eosin (HE) merged with DAPI (D).

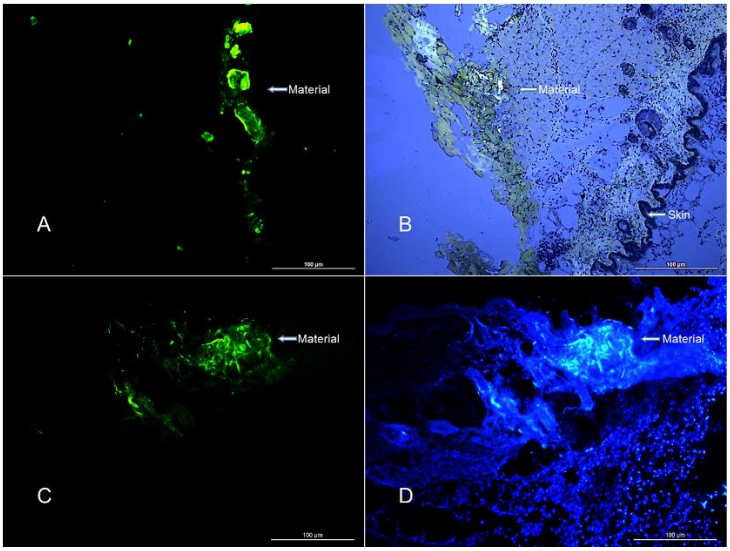

Fig. 10 Fluorescent images of rapidly frozen sections were gathered *via* inverted fluorescence microscopy. B shows image staining *via* haematoxylin and eosin (HE) merged with DAPI (D). The samples were harvested after 1 (A, B) and 3 months (C, D) of incubation.

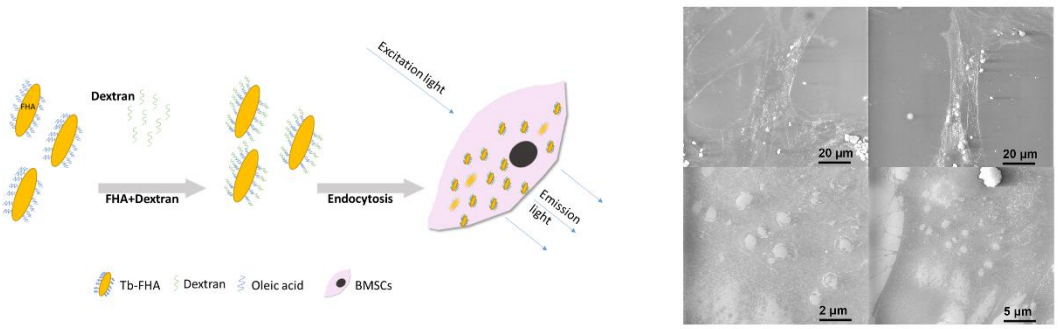

Scheme 1 Schematic showing dextran-coated fluorapatite nanorods doped with lanthanides in labelled bone marrow mesenchymal stem cells (BMSCs). ESEM results show dispersed agglomerations of nanorods on the cell surface; the white dots are the agglomerate nanorods.

Discussion

Fluorapatite nanorods doped with lanthanides were synthesised using the hydrothermal method. These nanorods possess excellent luminescent properties, uniform morphology, good crystallinity, uniformity of size and an agglomerate dispersed state in solution. When the surface of fluorapatite nanorods is coated with the surfactant of dextran, they change from a hydrophobic behaviour to hydrophilic behaviour. Hydrophilic behaviour can be used for biological imaging, drug delivery and other tissue engineering research. Bioactivity and degradation behaviour depend on the calcium to phosphorus atom molar ratio (Ca/P), crystallinity and phase purity. Fluorapatite nanorods have a Ca/P ratio of 1.67, which is equal to that of hydroxyapatite, an inorganic component of bone and tooth

enamel. Promising features of CaPs include their excellent bioactivity and biodegradability. The extracts of FHA cement caused no cytotoxicity in L929 cells, satisfied the relevant criterion for dental biomaterials, and demonstrated good cytocompatibility.[18,19]

Calcium phosphate nanoparticles, such as fluorapatite nanorods, as well as nano and micro hydroxyapatite particles can enhance the adhesion, proliferation, differentiation and mineralisation of bone marrow mesenchymal stem cells.[20-23] According to the real-time PCR results of ALP, Col-α1 and ON, the increased expression of the mRNA from the FHA group clearly demonstrates that fluorapatite nanorods that have been doped with lanthanides (Tb^{3+} or Eu^{3+}) can influence the differentiation of BMSCs. The following ELISA test also confirmed that rare earth elements do not influence fluorapatite nanorods in promoting the osteogenic differentiation of BMSCs. There is a synergistic effect of osteogenic differentiation between biochemical regents and fluorapatite nanorods.

In this article, dextran-coated fluorapatite nanorods doped with lanthanides proved to be successful in labelling and tracking cBMSCs *in vitro* and *in vivo*. Scheme 1 briefly demonstrates the process of nanorods entering BMSCs. ESEM results confirmed the existence of dispersed agglomerations of nanorods on the cell surface; the white dots are the nanorods. Nanorods enter BMSCs *via* endocytosis. They then become entrapped within the endosomes and released into the cytoplasm or trafficked to the acidic environments of the lysosomes for degradation.[18,24-26] Dextran is a type of cationic polymer that preferentially binds to early endosomes.[27] When dextran combines with nanorods, it can enhance the affinity of nanorods and cells and can contribute to the process of cell endocytosis. The existence of a receptor-mediated endocytosis pathway (or which receptor-mediated endocytosis pathway) remains unclear. An MTS assay demonstrated that the nanorods do not significantly influence cBMSC viability. This suggests that dextran-coated fluorapatite nanorods that have been doped with lanthanides have good biocompatibility, with and low cytotoxicity for BMSCs. Substituting fluorine into the HA lattice can increase crystallinity, leading to a reduced solubility for the FHA nanorods.[28] The fluorine substitution also improves thermal stability and other mechanical properties.[29] The above properties enable FHA nanorod resistance to degradation and stability in the cytoplasm. When the concentration of dextran-coated FHA- (Tb^{3+} or Eu^{3+}) nanorods in the solution is greater than 100 μg mL^{-1}, a small amount of crystal precipitation is visible. Thus, a concentration of 100 μg mL^{-1} is recommend; higher concentrations are ineffective.

Lanthanide complexes have a luminescence lifetime, from μs (Yb, Nd) to ms (Eu, Tb), which is significantly longer and more stable than the fluorescence lifetime of organic dyes, e.g., that for DAPI is 2.78 ns and for EGFP is 2.71 ns.[30] High photostability, high resistance to photobleaching, and a long luminescence lifetime make a large number of lanthanides complexes viable for live cell microscopy and *in vivo* imaging.[31,32] After HA nanorods doped with $Tb3^{+}$ are incubated with rabbit bone marrow mesenchymal stem cells in culture, the luminescence of the internalised HAP in the living cells was clearly observed under a fluorescent microscope. TEM analysis also confirmed the uptake of the particles by MSCs.[3]

Compared with organic fluorescent dyes, QDs have unique optical and electronic properties due to their sizes and compositions. They have fluorescence emissions that can be tuned to appear in visible to infrared wavelengths, large absorption coefficients across a wide spectral range and very high levels of brightness and photostability.[33] However, a great deal of concern has been voiced regarding the potential hazards of QDs due to their heavy metal content: some QDs may potentially cause DNA damage and promote carcinogenesis factors.[34-36] Luminescent fluorapatite nanorods are free of these heavy metal ions when compared with QDs and would not cause toxic reactions to cells or live

animals.[37] The organic fluorescent dyes CM-Dil and BrdU are usually used to track cells *in vivo*, but the tracing effect is difficult to achieve in 2 months.[38,39] The long-term (more than 3 months) *in vivo* experiments show that Tb-FHA nanorod-labelled BMSCs were involved in osteogenesis with the PCL scaffold.

Additionally, the surface modification of luminescent fluorapatite nanorods can be extended to many other similar approaches, such as those with protamine sulphate, chitosan or cellulose.[40-42] In our previous experiments, we used the TAT peptide as the surfactant and achieved good results; however, the TAT peptide-coated fluorapatite nanorods underwent decomposition and were inconvenient to store.[43] Dextran-coated fluorapatite nanorods doped with lanthanides are easy to synthesise, are accompanied by low costs, are simple to store, and have the potential to become an ideal tracer of BMSCs in bone tissue engineering.

Conclusion

We have demonstrated a facile hydrothermal method for the synthesis of fluorapatite nanorods doped with lanthanides. The hydrophobic surfaces of the nanorods were converted into hydrophilic surfaces with the surfactant of dextran. The rod-like nanoparticles showed excellent biocompatibility and strong luminescence and could be utilised for labelling and tracking BMSCs *in vitro* and *in vivo*. Labelled BMSCs were shown to reproducibly exhibit osteogenic differentiation potential in real-time PCR and ELISA assays. Long-term *in vivo* cell-tracking experiments confirmed the stability of dextran-coated Tb-FHA nanorods. In the present study, we validated a novel approach for labelling and tracking BMSCs in bone tissue engineering using dextran-coated fluorapatite nanorods doped with lanthanides, providing new prospects for nanorod use in biomedicine.

Acknowledgments

This project was supported by the National Basic Research Program of China (2012CB933903).

References

(1) Fox, K.; Tran, P. A.; Tran, N. Recent advances in research applications of nanophase hydroxyapatite. *ChemPhysChem* **2012**, *13*, 2495-2506.

(2) Chen, F.; Huang, P.; Zhu, Y. J.; Wu, J.; Zhang, C. L.; Cui, D. X. The photoluminescence, drug delivery and imaging properties of multifunctional Eu3+/Gd3+ dual-doped hydroxyapatite nanorods. *Biomaterials* **2011**, *32*, 9031-9039.

(3) Li, L.; Liu, Y.; Tao, J.; Zhang, M.; Pan, H.; Xu, X.; Tang, R. Surface modification of hydroxyapatite nanocrystallite by a small amount of terbium provides a biocompatible fluorescent probe. *The Journal of Physical Chemistry C* **2008**, *112*, 12219-12224.

(4) Zhang, C.; Yang, J.; Quan, Z.; Yang, P.; Li, C.; Hou, Z.; Lin, J. Hydroxyapatite nano-and microcrystals with multiform morphologies: Controllable synthesis and luminescence properties. *Crystal Growth and Design* **2009**, *9*, 2725-2733.

(5) Liu, H.; Chen, F.; Xi, P.; Chen, B.; Huang, L.; Cheng, J.; Shao, C.; Wang, J.; Bai, D.; Zeng, Z. Biocompatible fluorescent hydroxyapatite: synthesis and live cell imaging applications. *The Journal of Physical Chemistry C* **2011**, *115*, 18538-18544.

(6) Su, Y.; Hu, M.; Fan, C.; He, Y.; Li, Q.; Li, W.; Wang, L.-h.; Shen, P.; Huang, Q. The cytotoxicity of

CdTe quantum dots and the relative contributions from released cadmium ions and nanoparticle properties. *Biomaterials* **2010**, *31*, 4829-4834.

(7) Chen, N.; He, Y.; Su, Y.; Li, X.; Huang, Q.; Wang, H.; Zhang, X.; Tai, R.; Fan, C. The cytotoxicity of cadmium-based quantum dots. *Biomaterials* **2012**, *33*, 1238-1244.

(8) Hui, J.; Zhang, X.; Zhang, Z.; Wang, S.; Tao, L.; Wei, Y.; Wang, X. Fluoridated HAp: Ln3+ (Ln= Eu or Tb) nanoparticles for cell-imaging. *Nanoscale* **2012**, *4*, 6967-6970.

(9) Zhang, X.; Hui, J.; Yang, B.; Yang, Y.; Fan, D.; Liu, M.; Tao, L.; Wei, Y. PEGylation of Fluoridated HAp: Ln3+ Nanorods for Cell Imaging. *Polym. Chem.* **2013**.

(10) Sun, R.; Chen, K.; Wu, X.; Zhao, D.; Sun, Z. Controlled synthesis and enhanced luminescence of europium-doped fluorine-substituted hydroxyapatite nanoparticles. *CrystEngComm* **2013**, *15*, 3442-3447.

(11) Wang, X.; Li, Y. Synthesis and Characterization of Lanthanide Hydroxide Single‐Crystal Nanowires. *Angewandte Chemie International Edition* **2002**, *41*, 4790-4793.

(12) Hui, J.; Wang, X. Luminescent, Colloidal, F‐Substituted, Hydroxyapatite Nanocrystals. *Chemistry-A European Journal* **2011**, *17*, 6926-6930.

(13) Tassa, C.; Shaw, S. Y.; Weissleder, R. Dextran-coated iron oxide nanoparticles: a versatile platform for targeted molecular imaging, molecular diagnostics, and therapy. *Accounts of chemical research* **2011**, *44*, 842-852.

(14) Jang, H.; Ryoo, S.-R.; Kostarelos, K.; Han, S. W.; Min, D.-H. The effective nuclear delivery of doxorubicin from dextran-coated gold nanoparticles larger than nuclear pores. *Biomaterials* **2013**.

(15) Singh, S.; Dosani, T.; Karakoti, A. S.; Kumar, A.; Seal, S.; Self, W. T. A phosphate-dependent shift in redox state of cerium oxide nanoparticles and its effects on catalytic properties. *Biomaterials* **2011**, *32*, 6745-6753.

(16) Wilson, R.; Spiller, D. G.; Beckett, A.; Prior, I. A.; Sée, V. Highly stable dextran-coated quantum dots for biomolecular detection and cellular imaging. *Chemistry of Materials* **2010**, *22*, 6361-6369.

(17) Takemitsu, H.; Zhao, D.; Yamamoto, I.; Harada, Y.; Michishita, M.; Arai, T. Comparison of bone marrow and adipose tissue-derived canine mesenchymal stem cells. *BMC veterinary research* **2012**, *8*, 150.

(18) Bose, S.; Tarafder, S. Calcium phosphate ceramic systems in growth factor and drug delivery for bone tissue engineering: A review. *Acta Biomaterialia* **2012**, *8*, 1401-1421.

(19) Wei, J.; Wang, J.; Shan, W.; Liu, X.; Ma, J.; Liu, C.; Fang, J.; Wei, S. Development of fluorapatite cement for dental enamel defects repair. *Journal of Materials Science: Materials in Medicine* **2011**, *22*, 1607-1614.

(20) Hu, Q.; Tan, Z.; Liu, Y.; Tao, J.; Cai, Y.; Zhang, M.; Pan, H.; Xu, X.; Tang, R. Effect of crystallinity of calcium phosphate nanoparticles on adhesion, proliferation, and differentiation of bone marrow mesenchymal stem cells. *Journal of Materials Chemistry* **2007**, *17*, 4690-4698.

(21) Huang, Y.; Zhou, G.; Zheng, L.; Liu, H.; Niu, X.; Fan, Y. Micro-/Nano-sized hydroxyapatite directs differentiation of rat bone marrow derived mesenchymal stem cells towards an osteoblast lineage. *Nanoscale* **2012**, *4*, 2484-2490.

(22) Wang, X.; Zhang, Z.; Chang, S.; Czajka-Jakubowska, A.; Nor, J.; Clarkson, B.; Ni, L.; Liu, J. Fluorapatite Enhances Mineralization of Mesenchymal/Endothelial Co-cultures. *Tissue Engineering* **2013**.

(23) Samavedi, S.; Whittington, A. R.; Goldstein, A. S. Calcium phosphate ceramics in bone tissue engineering: A review of properties and their influence on cell behavior. *Acta Biomaterialia* **2013**.

(24) Liu, Z.; Zhang, Z.; Zhou, C.; Jiao, Y. Hydrophobic modifications of cationic polymers for gene delivery. *Progress in Polymer Science* **2010**, *35*, 1144-1162.

(25) Ferreira, L.; Karp, J. M.; Nobre, L.; Langer, R. New opportunities: the use of nanotechnologies to manipulate and track stem cells. *Cell stem cell* **2008**, *3*, 136-146.

(26) Bae, Y. M.; Park, Y. I.; Nam, S. H.; Kim, J. H.; Lee, K.; Kim, H. M.; Yoo, B.; Choi, J. S.; Lee, K. T.; Hyeon, T. Endocytosis, intracellular transport, and exocytosis of lanthanide-doped upconverting nanoparticles in single living cells. *Biomaterials* **2012**.

(27) Lencer, W. I.; Weyer, P.; Verkman, A. S.; Ausiello, D. A.; Brown, D. FITC-dextran as a probe for endosome function and localization in kidney. *American Journal of Physiology-Cell Physiology* **1990**, *258*, C309-C317.

(28) Shepherd, J. H.; Shepherd, D. V.; Best, S. M. Substituted hydroxyapatites for bone repair. *Journal of Materials Science: Materials in Medicine* **2012**, *23*, 2335-2347.

(29) Bianco, A.; Cacciotti, I.; Lombardi, M.; Montanaro, L.; Bemporad, E.; Sebastiani, M. F-substituted hydroxyapatite nanopowders: Thermal stability, sintering behaviour and mechanical properties. *Ceramics international* **2010**, *36*, 313-322.

(30) Berezin, M. Y.; Achilefu, S. Fluorescence lifetime measurements and biological imaging. *Chemical reviews* **2010**, *110*, 2641-2684.

(31) Bünzli, J.-C. G. Lanthanide luminescence for biomedical analyses and imaging. *Chemical reviews* **2010**, *110*, 2729-2755.

(32) Probst, J.; Dembski, S.; Milde, M.; Rupp, S. Luminescent nanoparticles and their use for in vitro and in vivo diagnostics. *Expert review of molecular diagnostics* **2012**, *12*, 49-64.

(33) Resch-Genger, U.; Grabolle, M.; Cavaliere-Jaricot, S.; Nitschke, R.; Nann, T. Quantum dots versus organic dyes as fluorescent labels. *Nature methods* **2008**, *5*, 763-775.

(34) Yong, K.-T.; Law, W.-C.; Hu, R.; Ye, L.; Liu, L.; Swihart, M. T.; Prasad, P. N. Nanotoxicity assessment of quantum dots: from cellular to primate studies. *Chemical Society Reviews* **2013**, *42*, 1236-1250.

(35) Wang, Y.; Hu, R.; Lin, G.; Roy, I.; Yong, K.-T. Functionalized Quantum Dots for Biosensing and Bioimaging and Concerns on Toxicity. *ACS applied materials & interfaces* **2013**, *5*, 2786-2799.

(36) Tsoi, K. M.; Dai, Q.; Alman, B. A.; Chan, W. C. Are quantum dots toxic? Exploring the discrepancy between cell culture and animal studies. *Accounts of Chemical Research* **2012**, *46*, 662-671.

(37) Montazeri, N.; Jahandideh, R.; Biazar, E. Synthesis of fluorapatite–hydroxyapatite nanoparticles and toxicity investigations. *International journal of nanomedicine* **2011**, *6*, 197.

(38) Lequeux, C.; Oni, G.; Mojallal, A.; Damour, O.; Brown, S. A. Adipose derived stem cells: efficiency, toxicity, stability of BrdU labeling and effects on self-renewal and adipose differentiation. *Molecular and cellular biochemistry* **2011**, *351*, 65-75.

(39) Froelich, K.; Steussloff, G.; Schmidt, K.; Technau, A.; Scherzed, A.; Hackenberg, S.; Radeloff, A.; Hagen, R.; Kleinsasser, N. DiI Labeling of Human Adipose-Derived Stem Cells: Evaluation of DNA Damage, Toxicity and Functional Impairment. *Cells Tissues Organs* **2013**, *197*, 384-398.

(40) Lobov, S. A.; King, D. W.; Knox, K. J.; Senden, T. J.; Stephens, R. W. Cationised radiolabelled nanoparticles for perfusion imaging of the lungs. *Biomaterials* **2012**.

(41) Majedi, F. S.; Hasani-Sadrabadi, M. M.; Emami, S. H.; Shokrgozar, M. A.; VanDersarl, J. J.; Dashtimoghadam, E.; Bertsch, A.; Renaud, P. Microfluidic assisted self-assembly of chitosan based nanoparticles as drug delivery agents. *Lab on a Chip* **2013**, *13*, 204-207.

(42) Wu, J.; Zhao, N.; Zhang, X.; Xu, J. Cellulose/silver nanoparticles composite microspheres: eco-

friendly synthesis and catalytic application. *Cellulose* **2012**, *19*, 1239-1249.

(43) Pan, L.; He, Q.; Liu, J.; Chen, Y.; Ma, M.; Zhang, L.; Shi, J. Nuclear-targeted drug delivery of TAT peptide-conjugated monodisperse mesoporous silica nanoparticles. *Journal of the American Chemical Society* **2012**, *134*, 5722-5725.